Time-resolved terahertz time-domain near-field microscopy

Research Article | Vol. 26, No. 24 | 26 Nov 2018 | OPTICS EXPRESS 32118
Optics EXPRESS

Time-resolved terahertz time-domain near-field microscopy

N. J. J. van Hoof,[1,2,*] S. E. T. ter Huurne,[2] J. Gómez Rivas,[1,2] and A. Halpin[1]

[1] *Dutch Institute for Fundamental Energy Research – DIFFER, De Zaale 20, 5612 AJ, Eindhoven, Netherlands*
[2] *Department of Applied Physics and Institute for Photonic Integration, Eindhoven University of Technology, 5600 MB, Eindhoven, Netherlands*
[*] *n.j.j.hoof@tue.nl*

Abstract: We demonstrate a novel method for measuring terahertz (THz) photoconductivity of semiconductors on length scales smaller than the diffraction limit at THz frequencies. This method is based on a near-field microscope that measures the transmission of a THz pulse through the semiconductor following photoexcitation by an ultrafast laser pulse. Combining back-excitation of the sample using a Dove prism, and a dual lock-in detection scheme, our microscope design offers a flexible platform for near-field time-resolved THz time-domain spectroscopy, using fluences available to typical laser oscillators. Experimental results on a thin film of gallium arsenide grown by metal organic chemical vapor deposition are presented as a proof-of-concept, demonstrating the ability to map the complex conductivity as well as sub-ps dynamics of photoexcited carriers with a resolution of $\lambda/10$ at 0.5 THz.

1. Introduction

Terahertz time-domain spectroscopy (THz-TDS) has become a widely adopted experimental technique for the investigation of material properties in the far-infrared region of the electromagnetic spectrum [1]. THz-TDS can be used to extract the high-frequency complex conductivity of materials over a large bandwidth, without the need of electrical contacts [2], allowing to extract carrier mobilities in a non-invasive manner. Additionally, broadband THz sources can be combined with ultrashort excitation pulses to study transient photoconductivity in semiconductors [3], extending the scope of THz-TDS to study the dynamics of carrier relaxation in materials of optoelectronic relevance. This technique, known as time-resolved THz spectroscopy (TRTS), is typically realized using a THz time-domain spectrometer, where the differential transmission of THz pulses through an optically excited sample is measured by electro-optic sampling [4, 5]. Pioneering work on conventional semiconductors [3, 6] have demonstrated the strength of TRTS, and paved the way for more recent investigations of novel systems such as graphene [7] and (2D)-semiconductors [8, 9], as well as molecular [10] and nanowire systems [11].

However, in spite of the many advantages offered by THz spectroscopy for characterizing materials, the use of THz radiation presents an important challenge, namely the diffraction limit: the smallest possible spot size achievable using conventional optics leads to a beam waist diameter on the order of millimeters for the longest wavelengths employed in typical experiments [12]. For the case of photoexcited samples, this calls both for large homogeneous samples and wide-area excitation beams. In typical TRTS experiments the sample is analyzed as an effective medium, therefore the contribution of defects in the sample will be averaged over the area covered by the diffraction-limited THz probe spot. Moreover, the latter condition of wide-field photoexcitation is equally important to ensure homogeneous generation of charge carriers across the probed sample area [6, 13]. Fabrication of large samples is not always feasible and electrical measurements can be equally impractical [8, 14]. Furthermore large excitation spot sizes with the necessary fluence for conducting TRTS typically restricts these experiments to expensive amplified laser systems.

#342504 https://doi.org/10.1364/OE.26.032118
Journal © 2018 Received 16 Aug 2018; revised 5 Oct 2018; accepted 6 Oct 2018; published 20 Nov 2018

Optics EXPRESS

To address the aforementioned limitations set by diffraction, recent developments in the mid-infrared (MIR), THz and microwave spectral regions have turned to near-field microscopy. Near-field techniques probe spatial lengths much smaller than the diffraction limit, allowing to circumvent many of the challenges that complicate conventional TRTS. Implementations of steady-state (photo-)conductivity mapping range from scattering near-field microscopy using sharp tips [15–19], to experiments relying on microwaves or narrow band THz sources [20, 21]. However, transient photoconductivity near-field measurements at THz frequencies have until recently remained largely unexplored [22, 23].

In this manuscript, we demonstrate an implementation of time-resolved THz near-field (TR-THz-NF) microscopy for determining the complex conductivity and carrier dynamics of photoexcited semiconductors over areas much smaller than the diffraction limit at THz frequencies. We measure the photoconductivity and carrier dynamics of a thin layer of gallium arsenide (GaAs) grown by metal organic chemical vapor deposition (MOCVD) by combining a near-field THz detector, based on a broadband micro-structured photoconductive antenna [24] with sub-ps optical pulses generated by a fiber oscillator for photoexcitation. These measurements reveal differences in carrier dynamics on length scales significantly smaller than the wavelength at THz frequencies. We will first describe the instrument, providing the details on the acquisition scheme of the THz near-field transmission, before presenting the measurements on the thin layer of GaAs.

2. Instrument design

The time-resolved THz near-field (TR-THz-NF) microscope is developed from a commercially available coaxial far-field THz-TDS system (Menlosystems GmbH, TeraK15). A schematic representation of the microscope is shown in Fig. 1. This spectrometer has an Er-doped fiber laser operating at 1560 nm which produces a train of 100 fs long pulses at a repetition rate of 100 MHz with an average power of 500 mW. Approximately 20 mW of this optical power is sent to an InGaAs/InAlAs photoconductive antenna generating a train of THz pulses at the same repetition rate. The generated spectrum is centered at 1.5 THz with a bandwidth of approximately 3 THz. The remaining light is frequency doubled to 780 nm and is used both for photoexcitation, and the near-field detection of the transmitted THz pulses through the sample.

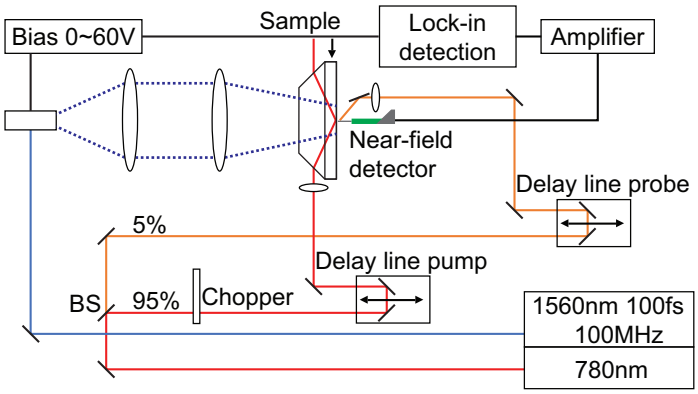

Fig. 1. Schematic representation of the TR-THz-NF microscope. The addition of a Dove prism allows to perform spatially dependent time-resolved differential transmittance measurements. The red line denotes the pump beam that excites the sample, a beam splitter (BS) splits of a small portion of the power to probe THz transients using the near-field detector (orange line). The THz emitter is excited by the light blue line resembling a fiber carrying 1560nm light to generate a THz beam (dashed blue line) which is collected and focused onto the sample using lenses.

Optics EXPRESS

The near-field detection relies on a micro-structured photoconductive antenna design (Protemics GmbH, TeraSpike TD-800-X). These photoconductive microprobes consist of a small and thin layer of low-temperature grown GaAs (LT-GaAs) with gold electrodes. The 780 nm pulse (optical probe 5 mW) is focused at the 10 μm gap between the electrodes where it excites the LT-GaAs and creates a transient population of excited carriers in the gap. The impinging THz field accelerates these short-lived charges towards the electrodes, leading to a photocurrent with amplitude and sign proportional to the electric field at the location of the photoexcited microprobe at the time of excitation. The orientation of gap between the electrodes relative to the THz field allows for the separation of independent polarization components in the THz near-field [25]. The timing between the optical probe and the THz pulse is given by a computer controlled delay stage (Newport, M-ILS150CCL), allowing to sample the THz waveform in the time-domain as in conventional THz-TDS systems. The electrical bias for the THz generation on the emitter is modulated at a frequency of 1500 Hz to generate a differential photocurrent that is amplified and detected using a lock-in amplifier (Ametek, SR-7270) to suppress dark current and reduce noise.

The majority (95%) of the 100 fs long 780 nm pulses are sent through an additional delay stage towards the sample for photoexcitation. Upon arrival, this pump pulse will induce a population of free-carriers, which will absorb the incoming THz radiation. The large angle under which the pump pulse excites the sample stretches the pulse to ≈300 fs, which sets the upper limit in temporal resolution. A mechanical chopper (Newfocus, 3501) that is phase-locked to the modulation of the THz, modulates the pump at a frequency of 1 kHz to evaluate the THz near-field measured at the sample with and without pumping in rapid succession. This modulation, together with that of the THz emitter, allows for self-referenced differential transmission measurements [26, 27]. The advantage of this dual modulation detection scheme is that it simultaneously records both the absolute THz intensity through the excited and unexcited sample, I_{pump} and I_0 respectively. The ratio of these intensities will be referred to as the transmittance $T = I_{\text{pump}}/I_0$. A detailed description of the modulation scheme that enables this simultaneous self-referenced detection can be found in the Appendix.

The introduction of the pump beam to the near-field microscope poses an important challenge: its intensity is sufficient to permanently damage the fragile THz microprobe, which is positioned in close proximity to the surface of the sample. Therefore, we cannot focus the pump beam onto the front of the sample, where scattered light would directly damage the probe. Back excitation in this case only partially addresses the problem, as the sample must then be optically thick at

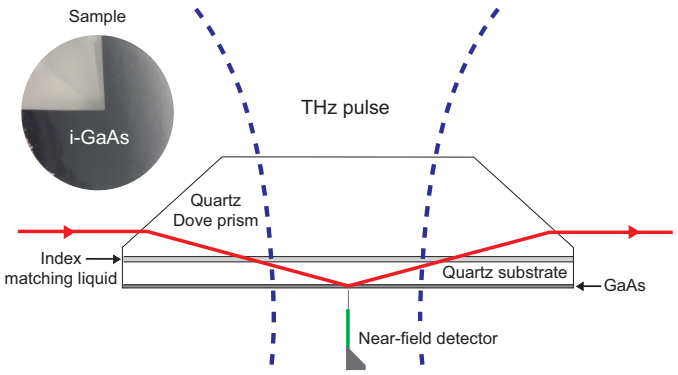

Fig. 2. Schematic representation of the total internal reflection configuration designed for combining a pump beam with the THz microprobe detector. The Dove prism ensures that the pump beam hits the interface at the probe position under an angle larger than the critical angle to suppress transmission of the large pump fluence towards the detector. Inset: Photograph of the sample.

Optics EXPRESS

the excitation frequency to avoid damage due to residual transmission of the excitation pulses. Moreover, scanning over defects or edges will still result in permanent damage to the THz microprobe.

We solve this problem by exciting the sample in a total internal reflection configuration. For this purpose, we use a z-cut quartz prism as schematically illustrated in Fig. 2. This prism has the shape of a truncated right-angle prism (Dove prism). The top of the prism presents a flat surface to the incoming THz beam, reducing the geometrical distortion that would otherwise occur. The pump beam, meanwhile, is incident from one of the side facets of the Dove prism and directed towards the rear part of the sample under an angle larger than the critical angle for total internal reflection. This beam will be partially absorbed by the sample, and the fraction which is not absorbed is directed back into the prism and does not reach the photoconductive microprobe. The microprobe, THz pulse, and excitation spot together define the optical axis of the instrument. The sample is brought into contact with the prism using a thin layer of index matching liquid to ensure optical contact, while facilitating the parallel movement of the sample with respect to the interface of the Dove prism. The THz pulse is incident onto the sample at normal incidence through the Dove prism. In order to maintain the photoexcited area along the optical axis, the sample moves in the x-y plane perpendicular to the near-field detector with the help of computer controlled stages (Newport, M-ILS150HA). This enables the spatial mapping of the transmitted THz electric near-field while the sample undergoes photo-excitation. Note that the sample is the only component moving during such a scan and that the prism is kept stationary.

3. Measurements

The TR-THz-NF microscope was used to measure the carrier recombination dynamics of photo-excited GaAs using the near-field probe close to the surface to detect the transmitted THz radiation with a sub-picosecond time resolution. These proof-of-principle measurements have been done on an unpassivated thin-film (3 μm thickness) of intrinsic GaAs on a 1 mm thick quartz substrate. The film was grown on top of a 2 inch GaAs(001) wafer with a sacrificial AlAs layer in between by MOCVD [28]. The GaAs film was transferred from the wafer by selective etching of the AlAs layer and bonding the thin-film to a 1 mm thick quartz substrate using a mercapto-ester polymer [29]. One-fourth of the GaAs wafer was removed to leave an edge for spatial mapping and referencing purposes. A photograph of the sample is shown in the inset of Fig. 2.

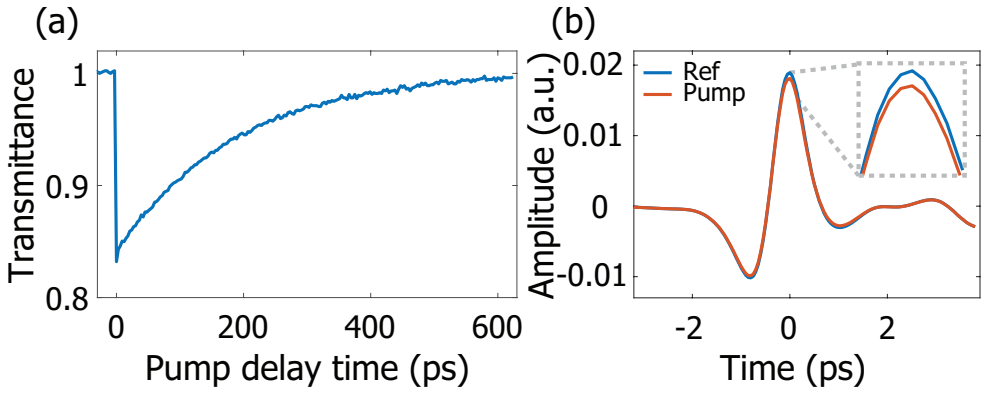

Fig. 3. (a) THz transmittance through photoexcited GaAs as a function of pump delay time, for a probe delay corresponding to the peak THz field amplitude, corresponding with Time=0 in (b). (b) Referenced and pumped transients, showing the difference in field amplitudes of which the ratio is the square root of the transmittance $T^{\frac{1}{2}}$.

Optics EXPRESS

The dynamics of photoexcited carriers can be recorded by probing the THz transmittance T as a function of pump arrival time. Figure 3(a) shows such a measurement, where we observe an initial 15% reduction in THz transmittance upon photoexcitation, induced by an absorbed fluence of 56.7 μJ/cm^2 in an optical focus with a radius of 25μm. By changing the delay between the optical pump and the THz probe, we measure a carrier lifetime of τ = 155 ps, associated with the thin layer of unpassivated GaAs, which is sensitive to surface defects [30]. For optimal contrast, we set the probe delay such that we are measuring the change in transmittance at the peak amplitude of the THz transient, shown in Fig. 3(b). The dynamic range of this instrument allows to reliably extract changes in transmittance on the order of 0.1% or a signal to noise ratio of 1000. This is achievable through the implementation of a self-referencing dual-modulation detection scheme, as well as by leveraging inexpensive yet robust fiber oscillator technology. For more details see the Appendix.

Thin samples, such as the one under investigation, are prone to inhomogeneities and defects that will locally alter the carrier recombination dynamics. Local variations in material properties can change the differential transmittance in both modulation depth and dynamics. Inhomogeneities are averaged out by the large area excitation/detection, inherent to far-field THz setups [31]. However, by scanning the sample in between the near-field probe and the THz beam, we can spatially resolve the carrier recombination dynamics with a sub-diffraction resolution.

A spatially dependent time-resolved differential transmittance measurement has been performed and is shown in Fig. 4. The GaAs sample is displaced by 800 μm along a line in 40 steps, scanning from the thin-film GaAs over an edge onto the quartz substrate, and recording the photoexcited carrier dynamics along this line. Figure 4(a) shows the transition between the GaAs film and the quartz substrate, where the grey dash-dotted line indicates the edge of the film. Above this line (x>600μm) the probe is on quartz and the transmittance goes to unity. On the quartz no free carriers are created by the optical pump, so there is no difference between the excited I_{pump} and non-excited sample I_0.

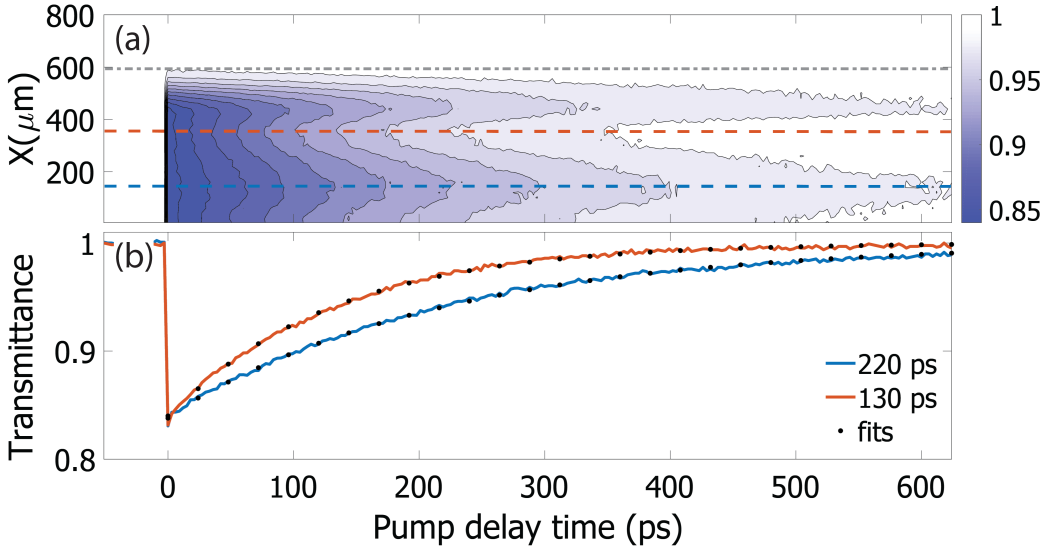

Fig. 4. (a) Time-resolved differential transmittance measurements along a straight line starting on GaAs and ending on the bare quartz substrate. The edge between the two regions is marked with a grey dashed-dotted line. (b) Two individual time-resolved differential transmittance measurements highlighting the variations in the decay time over sub-diffraction length scales, with their corresponding single exponential fits.

Optics EXPRESS

The spatially dependent photoinduced dynamics associated with free-carrier absorption in GaAs can be observed below the grey dashed-dotted line (x<600μm) in Fig. 4(a). Spatial variations are visible not only in the contrast between the quartz and GaAs, but also in the material quality of the GaAs itself, as indicated by the blue and red dashed lines. The decay of the excited carriers at the positions marked by these lines are shown Fig. 4(b). They indicate the longest (220 ps, blue curve) and shortest (130 ps, red curve) decay times measured, respectively. The significant difference at these two positions is likely caused by defects near the position marked by the red dashed line, which enhance the rate at which free carriers are trapped and thus shortens the carrier lifetime.

The results above demonstrate variations in the photoinduced response of the sample to THz radiation on length scales smaller than the wavelength. However, when building a microscope resolution is one of the most important properties to evaluate. The resolution of the TR-THz-NF microscope is established by scanning from GaAs towards a bare substrate, whilst collecting photoexcited time-domain transients. Fourier transforming these transients gives the spatial dependent transmittance as a function of frequency. Figure 5(a) shows the spatial dependence of the transmittance for 3 different frequencies during a scan over the edge between the GaAs and quartz located at the center of the scan. A resolution of 60±10 μm is obtained from the full width at half maximum of Gaussian fits performed through the spatial derivative as shown in Fig. 5(b), corresponding with a 10/90 criterion in the edge scan [32]. At the peak frequency of 0.5 THz, this corresponds to a spatial resolution of $\lambda/10$. This resolution is high enough to perform spectroscopy on small samples that would be close to impossible using far-field techniques. Please also note that the resolution is only limited by the near-field probe, and not by the size of the optical focus. As such this system could additionally be used with weakly focused or collimated excitation beams from an amplified laser system.

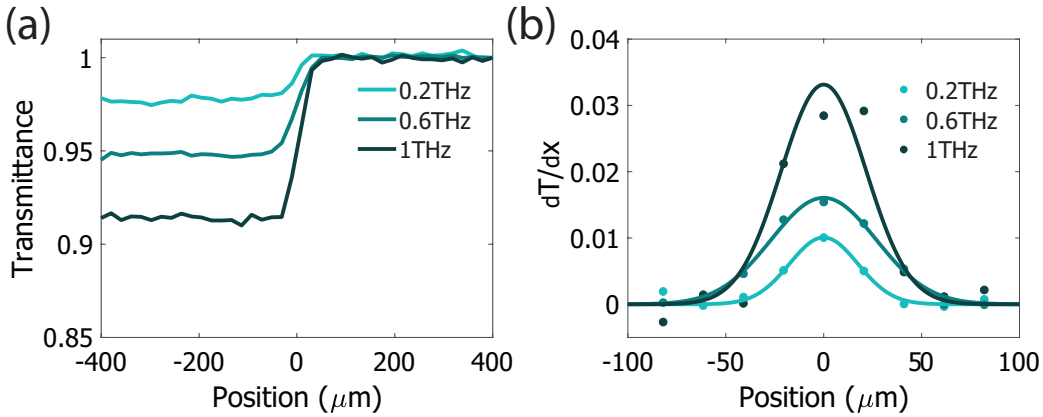

Fig. 5. (a) Spatial scan, recording the frequency dependent transmittance from GaAs to quartz. THz transients are measured 50 ps after the arrival of the optical pump pulse, these transients are Fourier transformed an plotted against their measured position for 3 frequencies. (b) Spatial derivative of the transmittance, fitted by Gaussians to give a FWHM of 60 ±10μm.

Unlike single frequency probes [33], this instrument can determine the complex conductivity over a broad bandwidth (0.4-1.1 THz). The carrier density and mobility can be obtained by relating the complex THz transmission through the photoexcited sample to the spectral dependence of the conductivity. The measured THz transmittance as a function of frequency is shown in Fig. 6. The transmission spectrum was measured 50 ps after photoexcitation and repeated 10 times to obtain confidence intervals. By measuring the complex THz transmission through the photoexcited samples in the time-domain, we can extract the carrier density and mobility through the spectral

Optics EXPRESS

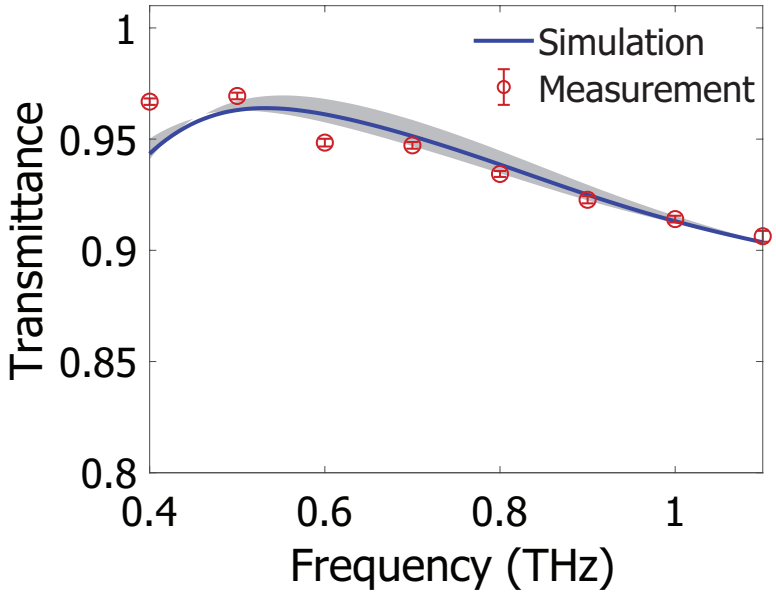

Fig. 6. Comparison between measured and simulated transmittance spectra of a GaAs photoexcited disk with a radius of 25 μm, on a thin layer (3 μm thick) with a carrier concentration of $1.25 \cdot 10^{16}$ cm^{-3} and a mobility of 3300 cm^{2}V^{-1}s^{-1}.

dependence of the conductivity.

A full wave simulation is conducted with a Finite-Difference Time-Domain (FDTD) simulation package (Lumerical) to reproduce the measured spectrum. The photoexcited system is represented by a 3μm thick dielectric disk with a radius of 25 μm, corresponding to the excited part of the GaAs film in the experiment. The carrier density N following photo-excitation is estimated to be $1.25 \cdot 10^{16}$ cm^{-3} based on an absorbed fluence of 56.7 μJ/cm^2, and a mobility μ_e of 3300 cm^{2}V^{-1}s^{-1}, in line with previously reported work on this sample [34].

This disk is placed inside a background medium of 3μm thick intrinsic GaAs with a THz plane wave impinging through the quartz substrate. The frequency dependent permittivity $\tilde{\epsilon}$ of the dielectric disk and background medium are calculated by using the Drude model to obtain the complex conductivity $\tilde{\sigma}$;

$$\tilde{\sigma}(\omega) = \frac{10^6 N e \mu_e}{1 - i\omega\tau}, \tag{1}$$

where, τ is the scattering time; ($\tau = m_e\mu_e/e$), with e as the elementary charge and m_e effective electron mass. Maxwell's equations are used to relate the complex conductivity to a complex permittivity;

$$\tilde{\epsilon}(\omega) = \epsilon_\infty + \frac{i\tilde{\sigma}}{\omega\epsilon_0}. \tag{2}$$

The simulated electric field parallel to the impinging polarization (co-polarized) is recorded in a plane 10 μm away from the surface, related to the location of the photoconductive gap in the microprobe itself. The electric near-field is averaged over a disk with a diameter of 60 $\pm$10μm, to account for the finite detection area of the microprobe, which was determined from Fig. 5. The resulting spectrum is divided by an identically processed simulation without the excited disk, (only the intrinsic GaAs film on top of the quartz substrate) to yield the frequency dependent transmittance. As a result of the finite uncertainty in the detection area, we depict the calculated

Optics EXPRESS

transmittance together with a confidence interval (grey shade around the mean (blue curve), shown together alongside the experimental transmittance spectra in Fig. 6.

The simulations reproduce the experimental results for frequencies between 0.6 and 1 THz with the input parameters as stated above. In simulations with higher carrier densities we start to approach the plasma frequency in GaAs, leading to the creation of a localized plasmonic resonance. However, the fluence of the optical pump using our current source was not sufficient to explore active THz plasmonics [34].

4. Conclusion

We have demonstrated an implementation of Time-Resolved THz near-field spectroscopy using microprobes, which achieve a spatial resolution of 60 μm with sub-picosecond temporal resolution. By exploiting double lock-in detection a signal to noise ratio of 1000/1 was achieved, as transmittance differences of 0.1% are observable and measurable. A prism based excitation geometry was introduced to shield the microprobes from damage, while maintaining the possibility to pump the sample with high fluence sources. While we employ a fiber oscillator and low pulse energies for the measurements above, the basic design of this instrument allows for its combination with pulsed lasers operating at various repetition rates and wavelengths.

These combined results enable scanning measurements of local perturbations in the transmittance of the THz fields associated with photoexcited carriers in small semiconducting samples. As a proof-of-concept, we demonstrate spatially varying carrier lifetimes, alongside THz transmission spectra, revealing the spectral response of photoinduced carriers in GaAs. In this manner, we are able to extract both recombination dynamics of carriers, but also the mobilities of photoexcited carriers, without needing to photoexcite samples over large areas. We thus expect that this approach will provide a useful platform for investigating the spatial dependence of photoconductivity in novel materials for opto-electronics.

Appendix

A dual modulation technique has been used in static and time-resolved THz spectroscopy (TRTS) for noise reduction in differential scans [26, 27]. Double modulation lock-in detection for TRTS uses two different frequencies, one for modulating the THz signal and the other for the modulation of the optical pump. These frequencies cannot be sub-harmonic with respect to each other, otherwise beat frequencies will end up in either or both demodulated channels and create additional noise. Therefore, a ratio of 3/2 between the two frequencies is chosen. The modulation scheme is shown as a function of time in Fig. 7. The THz generation is modulated by periodically applying a bias voltage on the photoconductive antenna at a frequency of 1.5 kHz, denoted as M_1, while the pump is modulated by an optical chopper at a frequency of 1 kHz, denoted as M_2. The signal that is measured by the detector is shown in the bottom of Fig. 7. The signal will be equal to A_{ref} when the THz is on and the pump is off (shown as red blocks), and A_{pump} (shown as blue blocks) when both the THz and pump are on. The difference between these signals is defined as $\Delta A = A_{ref} - A_{pump}$.

The periodicity of this system is determined by the smallest common divider of the modulation frequencies. Therefore one period will contain three modulations of M_1 and two modulations of M_2. The signals related to these frequencies are labeled S_1 and S_2. Per period, S_1 will be comprised of $1.5A_{pump}$ and $1.5A_{ref}$ in the on state, and the off state will only contain dark counts. While S_2 will contain $1.5A_{pump}$ in the on state and $1.5A_{ref}$ in the off state. Since $A_{pump} = A_{ref} - \Delta A$ the signals in S_1 and S_2 will be given as:

$$S_1 = 1.5A_{ref} + 1.5A_{pump} = 3E_{ref} - 1.5\Delta A, \tag{3a}$$

$$S_2 = -1.5A_{ref} + 1.5A_{pump} = -1.5\Delta A. \tag{3b}$$

Optics EXPRESS

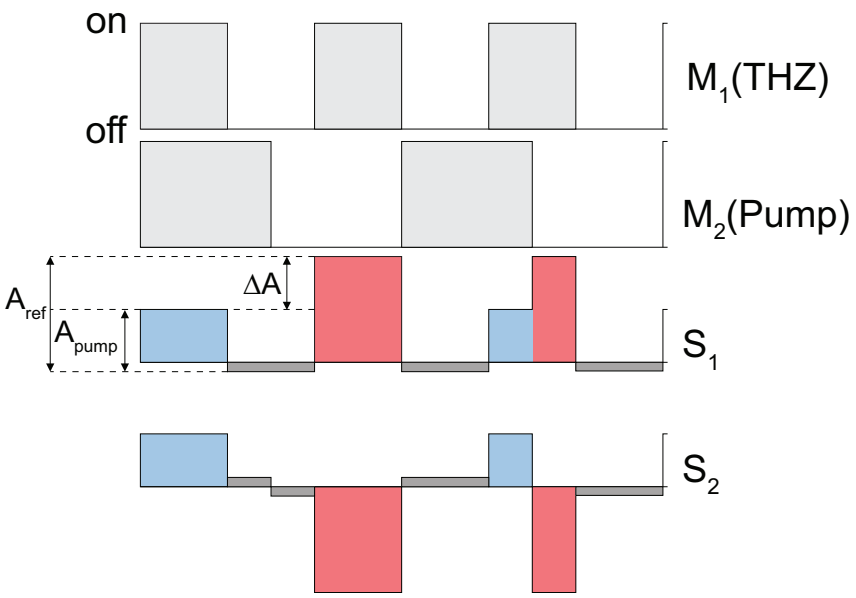

Fig. 7. Dual modulation detection scheme for simultaneous detection of pumped and reference states in a TRTS experiment.

The pumped and reference signals can be obtained from the two channels, $A_{pump} = (S_1 + S_2)/3$ and $A_{ref} = (S_1 - S_2)/3$. The noise reduction of the self-referencing measurement scheme is shown in Fig. 8. In Fig. 8(a) we can see the raw signals from a measurement with low excitation fluence, the signal is comparable to the noise floor. But the transmission defined as $T = A_{pump}/A_{ref}$, shows that differences as small as 0.1% are measurable (see Fig. 8(b)), due to the simultaneous detection scheme.

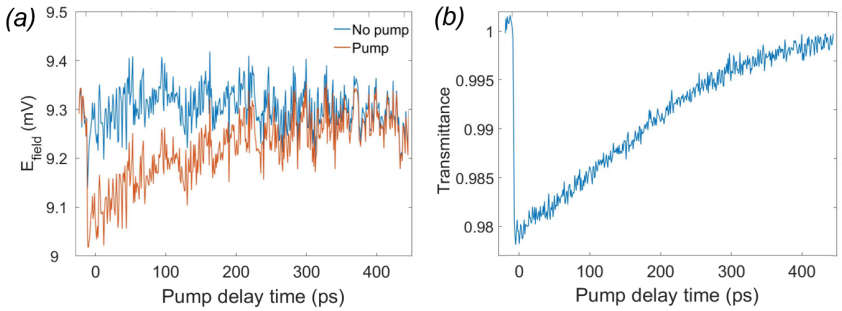

Fig. 8. (a) The raw signal of A_{ref} (blue) and A_{pump} (red) of a measurement with low excitation power. (b) The ratio of A_{pump}/A_{ref} plotted as a function of delay time, showing that sub-picosecond dynamics can be recorded up to a difference of only 0.1%.

Funding

Nederlandse Organisatie voor Wetenschappelijk Onderzoek (NWO) (680-47-628); NWO-Philips Industrial Partnership Program NanoPhotonics for Solid State Lighting; European Research Council (ERC) (259272, 665619).

Optics EXPRESS

Acknowledgments

We thank J. J. Schermer, G.J. Bauhuis, and P. Mulder for the fabrication of the sample.

Optics EXPRESS

References and links

1. R. Ulbricht, E. Hendry, J. Shan, T. F. Heinz, and M. Bonn, "Carrier dynamics in semiconductors studied with time-resolved terahertz spectroscopy," Rev. Mod. Phys. **83**, 543–586 (2011).
2. D. Grischkowsky, S. Keiding, M. van Exter, and C. Fattinger, "Far-infrared time-domain spectroscopy with terahertz beams of dielectrics and semiconductors," J. Opt. Soc. Am. B **7**, 2006–2015 (1990).
3. M. C. Beard, G. M. Turner, and C. A. Schmuttenmaer, "Transient photoconductivity in GaAs as measured by time-resolved terahertz spectroscopy," Phys. Rev. B **62**, 15764–15777 (2000).
4. Q. Wu and X. C. Zhang, "Free-space electro-optic sampling of terahertz beams," Appl. Phys. Lett. **67**, 3523–3525 (1995).
5. A. Nahata, A. S. Weling, and T. F. Heinz, "A wideband coherent terahertz spectroscopy system using optical rectification and electro-optic sampling," Appl. Phys. Lett. **69**, 2321–2323 (1996).
6. M. Schall and P. U. Jepsen, "Photoexcited GaAs surfaces studied by transient terahertz time-domain spectroscopy," Opt. Lett. **25**, 13–15 (2000).
7. J. D. Buron, D. H. Petersen, P. Bøggild, D. G. Cooke, M. Hilke, J. Sun, E. Whiteway, P. F. Nielsen, O. Hansen, A. Yurgens, and P. U. Jepsen, "Graphene conductance uniformity mapping," Nano Lett. **12**, 5074–5081 (2012).
8. C. J. Docherty, P. Parkinson, H. J. Joyce, M. H. Chiu, C. H. Chen, M. Y. Lee, L. J. Li, L. M. Herz, and M. B. Johnston, "Ultrafast transient terahertz conductivity of monolayer MoS2 and WSe2 grown by chemical vapor deposition," ACS Nano **8**, 11147–11153 (2014).
9. S. Kar, Y. Su, R. R. Nair, and A. K. Sood, "Probing photoexcited carriers in a few-layer MoS2 laminate by time-resolved optical pump-Terahertz probe spectroscopy," ACS Nano **9**, 12004–12010 (2015).
10. E. Knoesel, M. Bonn, J. Shan, F. Wang, and T. F. Heinz, "Conductivity of solvated electrons in hexane investigated with terahertz time-domain spectroscopy," J. Chem. Phys. **121**, 394–404 (2004).
11. H. J. Joyce, S. A. Baig, P. Parkinson, C. L. Davies, J. L. Boland, H. H. Tan, C. Jagadish, L. M. Herz, and M. B. Johnston, "The influence of surfaces on the transient terahertz conductivity and electron mobility of GaAs nanowires," J. Phys. D: Appl. Phys. **50**, 224001–224008 (2017).
12. M. Baillergeau, K. Maussang, T. Nirrengarten, J. Palomo, L. H. Li, E. H. Linfield, A. G. Davies, S. Dhillon, J. Tignon, and J. Mangeney, "Diffraction-limited ultrabroadband terahertz spectroscopy," Sci. Reports **6**, 1–7 (2016).
13. G. L. Dakovski, B. Kubera, S. Lan, and J. Shan, "Finite pump-beam-size effects in optical pump - terahertz probe spectroscopy," J. Opt. Soc. Am. B **23**, 139–141 (2006).
14. W. Choi, N. Choudhary, G. H. Han, J. Park, D. Akinwande, and Y. H. Lee, "Recent development of two-dimensional transition metal dichalcogenides and their applications," Mater. Today **20**, 116–130 (2017).
15. R. Hillenbrand, T. Taubner, and F. Keilmann, "Phonon-enhanced light matter interaction at the nanometre scale." Nature **418**, 159–162 (2002).
16. N. C. J. Van Der Valk and P. C. M. Planken, "Electro-optic detection of subwavelength terahertz spot sizes in the near field of a metal tip," Appl. Phys. Lett. **81**, 1558–1560 (2002).
17. H. T. Chen, R. Kersting, and G. C. Cho, "Terahertz imaging with nanometer resolution," Appl. Phys. Lett. **83**, 3009–3011 (2003).
18. F. Buersgens, R. Kersting, and H. T. Chen, "Terahertz microscopy of charge carriers in semiconductors," Appl. Phys. Lett. **88**, 112115–112117 (2006).
19. A. J. Das, R. Shivanna, and K. S. Narayan, "Photoconductive NSOM for mapping optoelectronic phases in nanostructures," Nanophotonics **3**, 19–34 (2014).
20. K. Dornich, N. Schüler, B. Berger, and J. R. Niklas, "Fast, high resolution, inline contactless electrical semiconductor characterization for photovoltaic applications by microwave detected photoconductivity," Mater. Sci. Eng. B **178**, 676–681 (2013).
21. C. Gao and X. D. Xiang, "Quantitative microwave near-field microscopy of dielectric properties," Rev. Sci. Instruments **69**, 3846–3851 (1998).
22. T. L. Cocker, V. Jelic, M. Gupta, S. J. Molesky, J. A. J. Burgess, G. D. L. Reyes, L. V. Titova, Y. Y. Tsui, M. R. Freeman, and F. A. Hegmann, "An ultrafast terahertz scanning tunnelling microscope," Nat. Photonics **7**, 620–625 (2013).
23. M. Eisele, T. L. Cocker, M. A. Huber, M. Plankl, L. Viti, D. Ercolani, L. Sorba, M. S. Vitiello, and R. Huber, "Ultrafast multi-terahertz nano-spectroscopy with sub-cycle temporal resolution," Nat. Photonics **8**, 841–845 (2014).
24. M. Wächter, M. Nagel, and H. Kurz, "Tapered photoconductive terahertz field probe tip with subwavelength spatial resolution," Appl. Phys. Lett. **95**, 41112–41114 (2009).
25. A. Bhattacharya and J. Gómez Rivas, "Full vectorial mapping of the complex electric near-fields of THz resonators," APL Photonics **1**, 86103–86110 (2016).
26. S. V. Frolov and Z. V. Vardeny, "Double-modulation electro-optic sampling for pump-and-probe ultrafast correlation measurements," Rev. Sci. Instruments **69**, 1257–1260 (1998).
27. K. Iwaszczuk, D. G. Cooke, M. Fujiwara, H. Hashimoto, and P. U. Jepsen, "Simultaneous reference and differential waveform acquisition in time-resolved terahertz spectroscopy." Opt. express **17**, 21969–21976 (2009).
28. J. J. Schermer, G. J. Bauhuis, P. Mulder, E. J. Haverkamp, J. van Deelen, A. T. J. van Niftrik, and P. K. Larsen, "Photon confinement in high-efficiency, thin-film III-V solar cells obtained by epitaxial lift-off," Thin Solid Films

Optics EXPRESS

511-512, 645–653 (2006).
29. M. M. A. J. Voncken, J. J. Schermer, A. T. J. van Niftrik, G. J. Bauhuis, P. Mulder, P. K. Larsen, T. P. J. Peters, B. de Bruin, A. Klaassen, and J. J. Kelly, "Etching AlAs with HF for epitaxial lift-off applications," J. Electrochem. Soc. **151**, G347–G352 (2004).
30. P. G. Huggard, J. A. Cluff, G. P. Moore, C. J. Shaw, S. R. Andrews, S. R. Keiding, E. H. Linfield, and D. A. Ritchie, "Drude conductivity of highly doped GaAs at terahertz frequencies," J. Appl. Phys. **87**, 2382–2385 (2000).
31. O. Mitrofanov, M. Lee, J. W. Hsu, L. N. Pfeiffer, K. W. West, J. D. Wynn, and J. F. Federici, "Terahertz pulse propagation through small apertures," Appl. Phys. Lett. **79**, 907–909 (2001).
32. J. F. Federici, O. Mitrofanov, M. Lee, J. W. P. Hsu, I. Brener, R. Harel, J. D. Wynn, L. N. Pfeiffer, and K. W. West, "Terahertz near-field imaging," Phys. Medicine Biol. **47**, 3727–3734 (2002).
33. F. Keilmann and R. Hillenbrand, "Near-field microscopy by elastic light scattering from a tip," Philos. Transactions Royal Soc. Lond. A **362**, 787–805 (2004).
34. G. Georgiou, H. K. Tyagi, P. Mulder, G. J. Bauhuis, J. J. Schermer, and J. Gómez Rivas, "Photo-generated THz antennas," Sci. Reports **4**, 1–5 (2014).